Struct Multidisc Optim
DOI 10.1007/s00158-017-1712-6

RESEARCH PAPER

Topology optimization of planar linkage mechanisms for path generation without prescribed timing

Sang Min Han[1] · **Suh In Kim**[1] · **Yoon Young Kim**[1]

Received: 26 November 2016 / Revised: 27 March 2017 / Accepted: 2 May 2017

Abstract The synthesis of planar linkage mechanisms by a topology optimization method has recently received much attention because both their numbers and dimensions can be simultaneously determined without baseline layouts. To synthesize a mechanism to produce a desired path at its end-effector, a desired path can be defined with or without prescribed timing. While earlier topology optimizations of mechanisms were all concerned with paths with prescribed timing, no study to deal with the topology optimization of mechanisms for path generation without prescribed timing is carried out in spite of its importance. The aim of this study is to propose and set up a gradient-based topology optimization formulation to synthesize planar linkage mechanisms that generate desired paths without prescribed timing. To this end, the desired path of the end-effector is expressed by the centroid distance function which is then represented by its Fourier descriptors. Then a topology optimization formulation using the Fourier descriptors is developed and the sensitivity analysis based on the Fourier descriptors is derived. Several numerical case studies are considered to verify the effectiveness of the proposed formulation. Some numerical issues appearing with the use of the Fourier descriptors are also investigated.

Keywords Planar linkage mechanism · Topology optimization · Fourier descriptors · Path generation without prescribed timing

1 Introduction

The purpose of path generation is to synthesize a mechanism that can convert an input motion to a motion following a desired path. Typically, the following three steps are used sequentially for mechanism synthesis: type synthesis by which the type of mechanism is defined; number synthesis by which the number of linkages and joints are determined; and dimensional synthesis by which the length of each linkage is calculated. Many mechanisms used today are developed through this process. On the other hand, there have been efforts trying to synthesize the number and dimension of a mechanism simultaneously. Kawamoto (2005) and Kawamoto et al. (2004a, b) proposed the concept of the topology optimization of mechanism synthesis using a nonlinear bar-based ground structure and succeeded in synthesizing short-path non-Grashof type linkages. Sedlaczek and Eberhard (2009) used a gradient-based optimization and genetic algorithm for mechanism synthesis using a nonlinear bar-based ground structure and succeeded in synthesizing large motion rigid body mechanisms. Ohsaki and Nishiwaki (2009) also proposed a two-stage general optimization approach for topology optimization of mechanism synthesis using a nonlinear bar-based ground structure. Rai et al. (2010) developed a unified procedure to synthesize planar linkage mechanisms that consisted of rigid and compliant bodies. Kim and Kim (2014) proposed an energy transmittance efficiency based topology optimization formulation, which has resolved the issue of satisfying the correct degree of freedom (DOF) of a rigid-body mechanism. In these

✉ Yoon Young Kim
yykim@snu.ac.kr

[1] School of Mechanical and Aerospace Engineering, Seoul National University, 1 Gwanak-ro, Gwanak-gu Seoul 151-742, Republic of Korea

Published online: 06 June 2017

studies, gradient-based optimizers are considered because of numerical efficiency and by the same reason, we will also consider using a gradient-based optimizer to update a candidate mechanism.

While the above-mentioned studies were mainly based on nonlinear-bar ground models, Kim et al. (2007) proposed a rigid block ground model. Specifically, the spring-connected rigid block model (SBM) was proposed in which a linkage mechanism is represented through the connectivity of each block. In the SBM based approach, zero-length variable-stiffness springs are introduced to connect rigid blocks. Later, Nam et al. (2012) dealt with numerical issues that could occur in the SBM and suggested some remedies. They also succeeded in synthesizing closed-loop complex path linkages. Using the SBM, Kim and Yoo (2014) also proposed a model that consists of deformable three blocks and can represent a revolute and prismatic joint. An extended version of the SBM (Kang et al. 2016) has been recently proposed to deal with more general joints.

In all studies mentioned above, a desired path is given with prescribed timing. This means that the end-effector should be located at a specific point for a specific time step or a specific location of an input actuator. In this case, closeness to the desired path is measured by the norm of the difference between the current end-effector location and the desired end-effector location at all given time steps. The norm over the whole time steps will be referred to as a structural error. In topology optimization of planar linkage mechanisms, the error can be used to form an objective function or a constraint equation. Therefore these approaches are equivalent to considering both the path shape and the prescribed timing. However, there are many situations where prescribed timing should be avoided. When timing prescription is not necessary or should be avoided, a different method to define the path error should be considered. Accordingly, a different topology optimization formulation should be developed which can compare only the path shape, but no related study has been conducted.

In order to perform the topology optimization of planar linkage mechanisms that generate paths without prescribed timing, we employ the centroid distance function to represent a path shape and express it in terms of the Fourier descriptors. These approaches have been extensively used for shape recognition (Bazan et al. 2009; Granlund 1972; Huang and Huang, 1998; Kauppinen et al. 1995; Lu and Sajjanhar 1999; Mehtre et al. 1997; Persoon and Fu 1977; Zahn and Roskies 1972; Zhang and Lu 2001). Also, several studies employed Fourier descriptors to define the path shape (Buśkiewicz 2010; Buśkiewicz et al. 2009; Ullah and Kota 1997; Wu et al. 2009; Wu et al. 2011) for shape optimization of linkage mechanisms. The main reasons to use the centroid distance function expressed in its Fourier descriptors are as follows. The centroid distance function (Yang et al. 2008) that is congruence-invariant does not require specific locations of the end-effector at specific times and the Fourier descriptors, in theory, are independent of how the centroid distance function is discretized along its arc length. More details will be given in Section 3.2. Accordingly, we develop a topology optimization formulation using the Fourier descriptors of the centroid distance function and perform necessary sensitivity analysis.

The outline of the paper is as follows. First, a brief introduction of the SBM will be given because our formulation will be based on the SBM. Then we present how the shape of the desired path of the end-effector can be described by the centroid distance function. Then, it will be expressed in terms of the Fourier descriptors. Because the Fourier descriptors are used to depict the desired path, the topology optimization formulation should be newly formulated by using the Fourier descriptors. To use a numerically efficient gradient-based optimizer, we must use continuously-varying design variables and in this study, the stiffness of block-connecting zero-length springs is controlled by the design variables. To update the design variables, we derive the sensitivities of the path-prescribing constraint equations expressed by the Fourier descriptors. The method of moving asymptotes (MMA) (Svanberg 1987) is used as a gradient optimizer. To check the validity of the proposed method, four design examples are conducted. The optimized results and iteration histories are examined for the considered numerical examples.

2 Modeling and analysis with a spring-connected rigid block model

2.1 Modeling

Figure 1(a) sketches a problem to synthesize a mechanism in a given design domain by a topology optimization for prescribed input and output motions. For the topology optimization of planar linkage mechanisms, a design domain must be discretized. Here, the spring-connected rigid block model (SBM) will be employed (Nam et al. 2012; Kim et al. 2007). In the SBM, the design domain is discretized into rigid blocks that are connected by artificial zero-length spring elements at their corners. Vertical and horizontal springs illustrated in the inset of Fig. 1(b) are introduced to connect adjacent blocks while oblique springs, called the anchoring springs, connect blocks to the ground. Depending on the stiffness values of the springs, two adjacent blocks can be perfectly connected or disconected at their common corner. (If the ground is viewed as an infiintley large block, this argument also applies to anchoring springs.)

To explain the correspondence between the stiffness values and the inter-block connectivity at a specific node, Fig. 2 is prepared. In all illustrations of Fig. 2, two blocks are connected at their common nodes (“left” and “right” nodes) by two

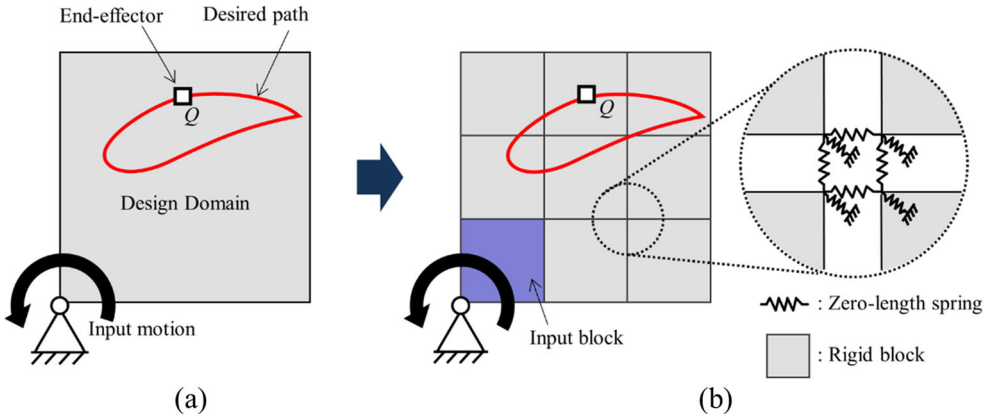

Fig. 1 Overview of the topology optimization based mechanism synthesis. (a) Problem definition and (b) ground model using spring-connected rigid blocks. In this illustration, the design domain is discretized into 9 blocks

block-connecting springs. They are also connected at ground by four anchoring springs. The stiffness values of block-connecting and anchoring springs will be denoted by k_c and k_a, respectively. These symbols will be also used to denote the zero-length springs. In the SBM approach, the stiffness coefficient of a zero-length spring is made to vary between $k_{\min}$ (lower bound) and $k_{\max}$ (upper bound).

As illustrated in Fig. 2, two interfacing rigid blocks can represent various connection states of two rigid links if the spring stiffness values reach their lower or upper bounds. For instance, if $k_c|_{left} = k_{\max}$, all other k_c and k_a's $= k_{\min}$, as in Fig. 2(a), the two blocks represent two links connected by a revolute joint. Similarly, if $k_c|_{left} = k_{\max}$, $k_a|_{left,\,lower} = k_{\max}$ and other k_c and k_a's $= k_{\min}$, as in Fig. 2(d), two blocks represent two links connected by a revolute joint grounded at the common left node location. (Here, 'lower' is used to indicate the anchoring springs attached to the lower block.) For more detailed accounts of the SBM and its extended model (called D-SBM), see Nam et al. (2012) and Kang et al. (2016). Note that during the topology optimization for mechanism synthesis, the stiffness values (k) are to vary continuously between $k_{\max}$ and $k_{\min}$ to allow the use of an efficient gradient-based optimizer. Because intermediate values of k should and will be suppressed, there is no need to interpret actual physical states corresponding to the intermediate cases.

2.2 Analysis

The motion of a mechanism using the spring-connected rigid block model can be analyzed by solving a quasi-static problem; if an input block is rotated by a certain angle at every time step, the positions of other blocks can be calculated. At each time step, the calculated positions of the blocks are so determined as to minimize the energy stored in the block-spring system subjected to a prescribed rotation of an input block (Kim et al. 2007). Therefore, we should first express the strain energy stored in the springs. Figure 3 illustrates a certain configuration of two blocks connected to each other by the ith block-connecting spring (k_{c_i}) and also connected to the ground by the jth anchoring spring (k_{a_j}). For the sake of

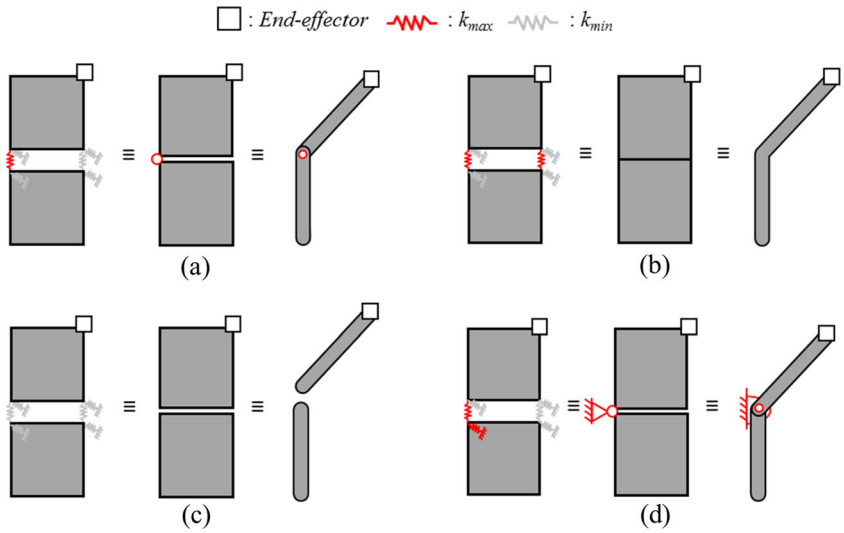

Fig. 2 Representation of different link connectivity depending on the stiffness values of k_c and k_a. (a) Connected by a revolute joint, (b) rigidly-connected, (c) disconnected and (d) connected by an anchored revolute joint

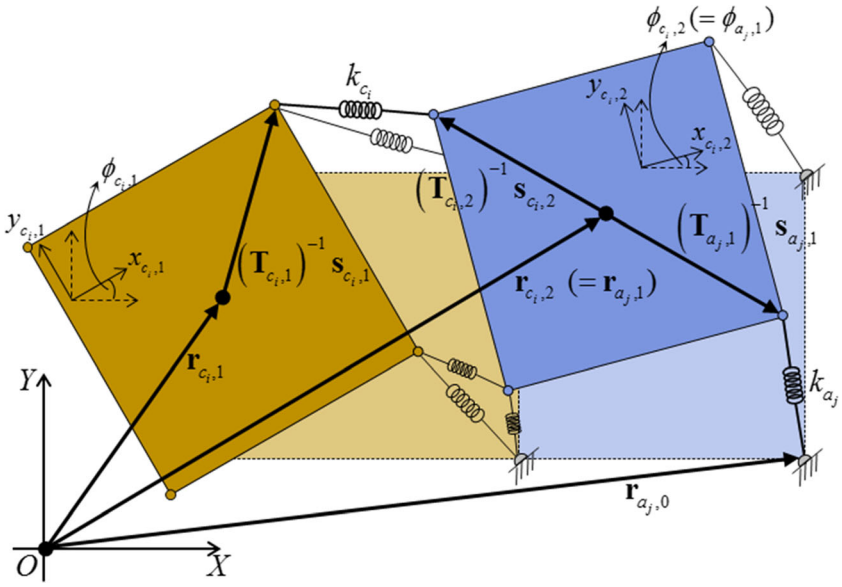

Fig. 3 Representation of two rigid blocks in motion

representation convenience, symbols "1" and "2" will be used to denote two rigid blocks connected by a block-connecting spring. On the other hand, symbol "0" is used to stand for the ground positions which are the same as the node positions of blocks at the zeroth optimization iteration step.

Let us consider k_{c_i} in Fig. 3. The center coordinates of two blocks connected by k_{c_i} are denoted by $\mathbf{r}_{c_i,1}$ and $\mathbf{r}_{c_i,2}$. If the relative distance from $\mathbf{r}_{c_i,1}$ ($\mathbf{r}_{c_i,2}$) to the k_{c_i} -attached corner of Block 1 (Block 2) in the local block-fixed coordinate system is denoted by $\mathbf{s}_{c_i,1}$ ($\mathbf{s}_{c_i,2}$), the displacement $\mathbf{u}_{c_i}$ experienced by the block-connecting spring k_{c_i} becomes

$$\mathbf{u}_{c_i} = \mathbf{r}_{c_i,1} + \left(\mathbf{T}_{c_i,1}\right)^{-1}\mathbf{s}_{c_i,1} - \mathbf{r}_{c_i,2} - \left(\mathbf{T}_{c_i,2}\right)^{-1}\mathbf{s}_{c_i,2} \tag{1}$$

The transformation matrices $\mathbf{T}_{c_i,1}$ and $\mathbf{T}_{c_i,2}$ are defined as

$$\mathbf{T}_{c_i,1} = \begin{bmatrix} \cos\phi_{c_i,1} & \sin\phi_{c_i,1} \\ -\sin\phi_{c_i,1} & \cos\phi_{c_i,1} \end{bmatrix};\quad \mathbf{T}_{c_i,2} = \begin{bmatrix} \cos\phi_{c_i,2} & \sin\phi_{c_i,2} \\ -\sin\phi_{c_i,2} & \cos\phi_{c_i,2} \end{bmatrix} \tag{2}$$

where $\phi_{c_i,1}$ (or $\phi_{c_i,2}$) denotes the angle between the global (X, Y) coordinate system and the local $(x_{c_i,1}, y_{c_i,1})$ (or $(x_{c_i,2}, y_{c_i,2})$) coordinate system. Likewise, the displacement of the jth anchoring spring (with respect to the ground) is given by

$$\mathbf{u}_{a_j} = \mathbf{r}_{a_j,1} + \left(\mathbf{T}_{a_j,1}\right)^{-1}\mathbf{s}_{a_j,1} - \mathbf{r}_{a_j,0} \tag{3}$$

In case of the anchoring spring, only one block, denoted by "1," is involved in the analysis of $\mathbf{u}_{a_j}$. The transformation matrix $\mathbf{T}_{a_j,1}$ is defined similarly to those in (2).

Accordingly, the motion analysis for the blocks can be solved as the following minimization problem:

$$\begin{aligned} &\underset{\mathbf{q}_{t^*}\in R^{3N_B}}{\text{Minimize}}\ E_{t^*}(\mathbf{q}_{t^*}) = U_{t^*}(\mathbf{q}_{t^*}) - W_{\text{out},t^*}(\mathbf{q}_{t^*}) \\ &= \sum_{i=1}^{N_c}\frac{1}{2}k_{c_i}(\mathbf{u}_{c_i})^T(\mathbf{u}_{c_i}) + \sum_{j=1}^{N_a}\frac{1}{2}k_{a_j}\left(\mathbf{u}_{a_j}\right)^T\left(\mathbf{u}_{a_j}\right) - W_{\text{out},t^*}(\mathbf{q}_{t^*}) \end{aligned} \tag{4}$$

where N_c and N_a denote the total number of the connecting springs and the total number of the anchoring springs, respectively. While U_{t^*} is the energy stored in the block-spring system, W_{out,t^*} denotes the work done by an external force. The force is intentionally introduced in order to define the energy transmittance efficiency which will be used as the objective function in the topology optimization formulation (explained later). The symbol $\mathbf{q}_{t^*}$ denotes the state variable vector at time t^* ($t^* = 1, 2, \cdots, T$) defined as

$$\mathbf{q}_{t^*} = \left\{\mathbf{q}_{1,t^*}^T, \mathbf{q}_{2,t^*}^T, \mathbf{q}_{3,t^*}^T, \cdots, \mathbf{q}_{N_B,t^*}^T\right\}^T \tag{5}$$

where

$$\mathbf{q}_{l,t^*} = \left\{\mathbf{r}_{l,t^*}, \phi_{l,t^*}\right\}^T = \left\{x_{l,t^*}, y_{l,t^*}, \phi_{l,t^*}\right\}^T \quad (l = 1, 2, \cdots, N_B) \tag{6}$$

Note that for the sake of convenience, $\mathbf{r}_{c_i,1}$ $\mathbf{r}_{c_i,2}$ and $\mathbf{r}_{a_j,1}$ are redefined as $\mathbf{r}_{l,t^*}$, the position vector of the lth block ($l = 1, 2, \cdots, N_B$ = the total number of rigid blocks) at a specific time step t^*. Also we will assume that $\phi_{c_i,1}$, $\phi_{c_i,2}$ and $\phi_{a_i,1}$ are redefined as $\phi_{l,t^*}(l = 1, 2, \cdots, N_B)$. When the lth block is an input actuation block A, $\mathbf{q}_{A,t^*} = \left[x_{A,t^*}, y_{A,t^*}, \phi_{A,t^*}\right]^T$, the state variable vector for the block, is considered to be prescribed. For example, if block 1 ($A = 1$) is an input block, a state variable vector

$\mathbf{q}_{1,t^*} = \left[x_{1,t^*}, y_{1,t^*}, \phi_{1,t^*}\right]^T$ is given. In this case, the total strain energy can be considered as a function of the remaining state variable vector $\mathbf{v}_{t^*}$, which is defined as

$$v_{t^*} = \left[\mathbf{q}_{2,t^*}^T, \mathbf{q}_{3,t^*}^T \cdots, \mathbf{q}_{N_B,t^*}^T\right]^T \tag{7}$$

The state variable vector ($\mathbf{q}_{t^*}$) can be obtained from (4), which can be solved by considering the force equilibrium of the SBM (see also Kang et al. 2016):

$$\frac{dE_{t^*}(\mathbf{q}_{t^*})}{d\mathbf{q}_{t^*}} = \mathbf{F}_{t^*}^{int}(\mathbf{q}_{t^*}) - \frac{dW_{t^*}(\mathbf{q}_{t^*})}{d\mathbf{q}_{t^*}} \tag{8}$$

$$= 0 \text{ for given } \mathbf{q}_{A,t^*} \left(t^* = 1, 2, \cdots, T\right)$$

where

$$\mathbf{F}_{t^*}^{int} = \frac{dU_{t^*}}{d\mathbf{q}_{t^*}} \tag{9}$$

In (8), $\mathbf{F}_{t^*}^{int}$ denote the internal force generated by springs. We will explain later how the external force is applied. As more details of the kinematic analysis can be found in Nam et al. (2012) or Kang et al. (2016), the explicit formula for $dU_{t^*}/d\mathbf{q}_{t^*}$ will not be given here.

3 Fourier based shape descriptors

This section is devoted to the description of a desired path without prescribed timing. Because all of earlier topology optimizations of linkage mechanisms have considered path generations only with prescribed timing, a method suitable to describe a desired path without prescribed timing is needed for the topology optimization formulation.

3.1 Structural error minimization for path description

When a path of an end-effector is desired with prescribed timing, the end-effector goes through the specified points at the prescribed time steps (Rattan 2009). In this case, mechanism synthesis can be performed by minimizing the structural error. Referring to Fig. 4(a), the structural error Ψ_{t^*} at time t^* is defined as $\Psi_{t^*} = \left\|\hat{\mathbf{r}}_{Q,t^*} - \mathbf{r}_{Q,t^*}\right\|$ where $\hat{\mathbf{r}}_{Q,t^*}$ is the specified position of the end-effector (its location is denoted by Q) at time t^* following a desired path and $\mathbf{r}_{Q,t^*}$ is the actual position of the end-effector at time t^*. By minimizing the summation of Ψ_{t^*} for all time steps, a mechanism to generate the desired path can be possibly synthesized. Figure 4(b) illustrates the process of mechanism synthesis topology optimization using the structural error. It indicates that the end-effector of the synthesized mechanism traces the specified points at the prescribed time steps. In actual design of mechanisms, it is difficult or undesirable to define the specific location of an end-effector at a specific time; there are many situations where only a desired path for an end-effector is given without prescribed timing. In this case, only the shape of the desired path that an end-effector traces matters. Therefore, a method to describe the path shape is needed and the topology optimization of a mechanism utilizing a selected description of the path shape should be formulated. This will be discussed in the next subsection.

3.2 Fourier description of the centroid distance function for path shape representation

In this section, we present a method to describe the desired path of the end-effector by using the Fourier descriptors of the centroid distance function in order to synthesize a mechanism tracing the desired path described without prescribed timing. This description has been used in pattern recognition (Bazan et al. 2009; Buśkiewicz 2010; Yang et al. 2008), but not employed in the topology optimization for mechanism synthesis. Here, we carry out the necessary analysis in order to implement the centroid distance function based Fourier description for the present topology optimizaiton.

Figure 5 gives some details of the centroid distance function based Fourier description and the reason why this description does not require prescribed timing. The variables needed to define the centroid distance function are depicted in Fig. 5(a). If a path is given, its centroid C located at (x_c, y_c) can be found as

$$x_c = \sum_{t^*=1}^{T} \frac{x_{t^*-1} + x_{t^*}}{2} \Delta\tilde{s}_{t^*}, y_c = \sum_{t^*=1}^{T} \frac{y_{t^*-1} + y_{t^*}}{2} \Delta\tilde{s}_{t^*} \tag{10}$$

where

$$\tilde{s}_{t^*} \sum_{j=1}^{t^*} \Delta\tilde{s}_j, \quad \Delta\tilde{s}_{t^*} = \frac{\left\|\mathbf{r}_{t^*} - \mathbf{r}_{t^*-1}\right\|}{L} \tag{11}$$

In (10, 11), (x_{t^*}, y_{t^*}) represent the coordinates of the t^*th point. The symbol $\Delta\tilde{s}_{t^*}$ denotes the dimensionless distance normalized by the total length of a given curve (L) between the(t^* - 1)th point and the t^*thpoint, and $\tilde{s}_{t^*}$ is the sum of the discretized arc lengths $\Delta\tilde{s}_{t^*}$ from the reference point to the t^*th point. The path is assumed to be described by the coordinates at its finite points. Now, one can write the centroid distance function f representing the distance from the centroid of the path to a generic point on it as

$$f\left(\tilde{s}_{t^*}\right) = \sqrt{\left(x\left(\tilde{s}_{t^*}\right) - x_c\right)^2 + \left(y\left(\tilde{s}_{t^*}\right) - y_c\right)^2} \tag{12}$$

In the subsequent discussion, the symbol $\tilde{s}_{t^*}$ will be denoted by $\tilde{s}$. If the centroid distance function is used, two curves can be viewed to be identical if they are congruent. For instance,

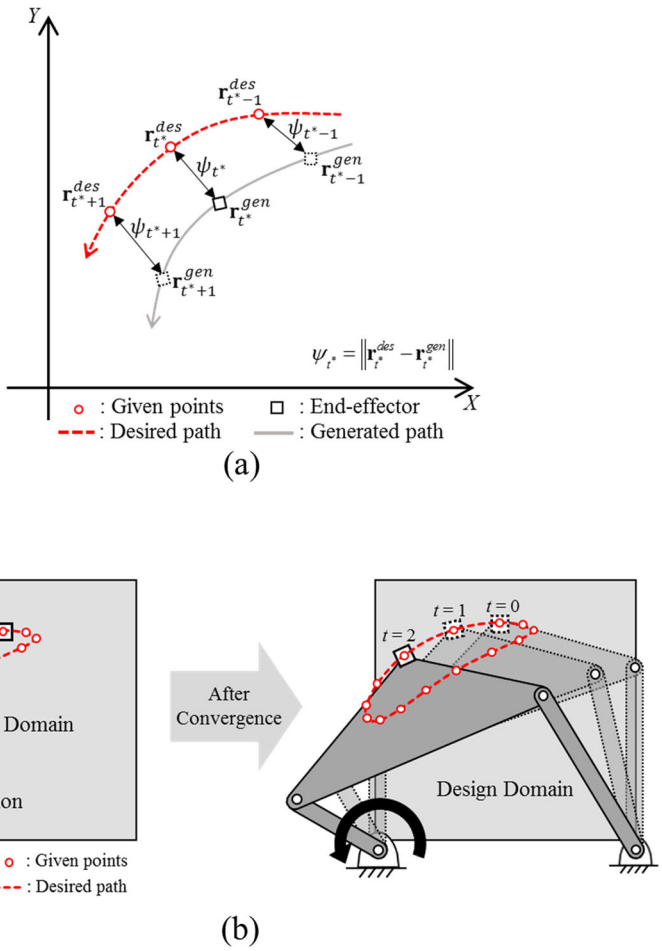

Fig. 4 The description of (a) the structural error at a specific time step when the current $\left(\mathbf{r}_{Q,t^*}\right)$ and desired $\left(\mathbf{r}_{Q,t^*}\right)$ locations of the end-effector Q are known and (b) the process of mechanism synthesis topology optimization using the structural error

even if the generated and desired paths have different centroids and orientations as in Fig. 5(b), they have the identical centroid distance function as illustrated in Fig. 5(c). Accordingly, the use of the centroid distance function allows the mechanism synthesis when the desired locations of the end-effector are not specified at prescribed timing.

In Fig. 5(c), the graph on the left shows the centroid distance functions of the two paths in Fig. 5(b). Although the two paths in Fig. 5(b) occupy different locations with different orientations, the centroid distance functions of two paths have the same shape as in Fig. 5(c). Thus, the comparison with the shapes of the two paths can be possible when using the centroid distance function. In other words, the mechanism synthesis for path generation is possible when the specified positions that the end-effector should go through at prescribed timing are not given. However, if the centroid distance function is described directly by their values at specific arc length values $(\tilde{s}_j)$ and these values are used for target path tracing (i.e., $|f^{gen}(\tilde{s}_j) - f^{des}(\tilde{s}_j)|$ is minimized), the synthesized results could be affected by the curve discretization along the arc length coordinate, which may be viewed as timing in the arc length. To avoid this disadvantage, the centroid distance functions are expressed in Fourier series and the Fourier coefficients of the desired and generated centroid distance functions are compared for path tracing. Therefore, we consider the following Fourier expansion of the centroid distance function $f(\tilde{s})$:

$$f\left(\tilde{s}\right) \approx a_0 + \sum_{n=1}^{p} \left[a_n \cos\left(2n\pi\tilde{s}\right) + b_n \sin\left(2n\pi\tilde{s}\right) \right] \tag{13}$$

where the Fourier coefficients (descriptors) a_0, a_n and b_n can be calculated as

$$a_0 = \sum_{t^*=1}^{T} f\left(\tilde{s}_{t^*}\right) \Delta\tilde{s}_{t^*},$$
$$a_n = 2 \sum_{t^*=1}^{T} f\left(\tilde{s}_{t^*}\right) \cos\left(2n\pi\tilde{s}_{t^*}\right) \Delta\tilde{s}_{t^*}, b_n = 2 \sum_{t^*=1}^{T} f\left(\tilde{s}_{t^*}\right) \sin\left(2n\pi\tilde{s}_{t^*}\right) \Delta\tilde{s}_{t^*} \tag{14}$$

If the highest term used in the Fourier series is p as in (13), the centroid distance function can be represented by using $2p + 1$ variables. The graph on the right in Fig. 5(c) shows that the centroid distance functions f^{gen} and f^{des} approximated by a finite number of the Fourier descriptors represent virtually the same shape. Figure 5(d) illustrates the process of the mechanism synthesis topology optimization using the proposed method. It suggests that a linkage mechanism that generates the identical shape of the desired path can be

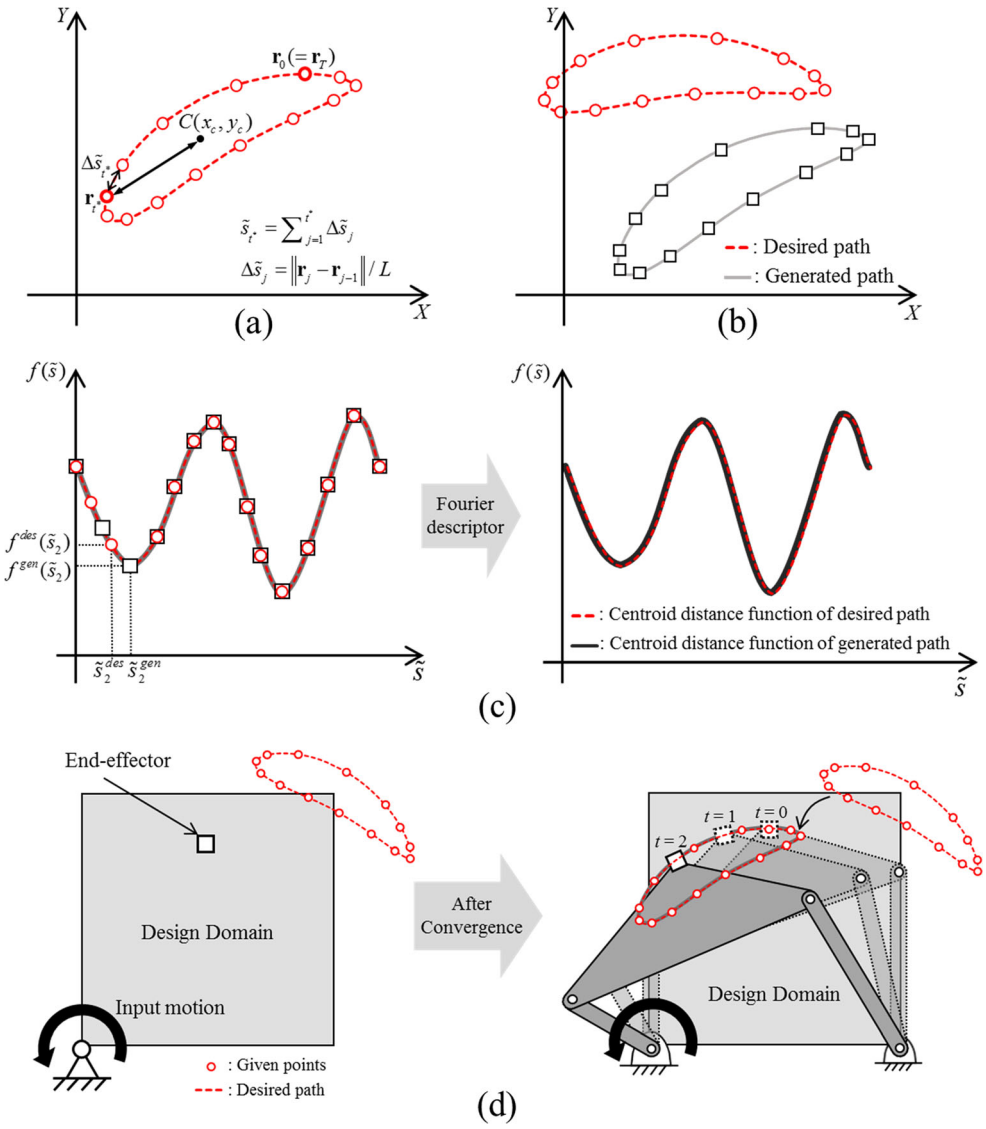

Fig. 5 (a) Variables needed to describe the centroid distance function $f(\tilde{s}_{t^*})$, (b) the desired and generated paths in different poses, (c) the desired $\left(f^{des}(\tilde{s}_{t^*})\right)$ and generated $\left(f^{gen}(\tilde{s}_{t^*})\right)$ centroid distance functions of the paths shown in (b) that are expressed in terms of their values at discrete points and expressed in the Fourier descriptors, and (d) the process of the mechanism synthesis topology optimization using the proposed centroid distance function based Fourier descriptors not requiring prescribed timing

synthesized even when its end-effector does not necessarily go through the specified points used to define the desired path. An illustrative synthesis problem demonstrating this aspect will be considered in Section 5.

4 Optimization formulation and sensitivity analysis

In this section, the topology optimization formulation suitable for the synthesis of a mechanism for a given path of its end-effector without prescribed times will be presented. Also, the sensitivity analysis will be performed, which should be available to update the design variables by a gradient-based optimizer.

4.1 Optimization formulation

As explained in Section 2.1, the configuration of a linkage can be found if the stiffness values of springs in the SBM are determined. When the stiffness of a spring reaches its maximum value $k_{\min}$, the spring represents the state of rigid connection at a node where two blocks are connected through. On the other hand, a disconnected state is represented if its stiffness value reaches its lower bound value $k_{\min}$. To be able to use a gradient-based optimizer, the stiffness value of the mth spring (either block-connecting or anchoring) is interpolated as a function of a dimensionless variable ξ_m, which is the mth design variable:

$$k_m = k_{\max} \times (\xi_m)^q \quad (0 \le \xi_m \le 1; m = 1, 2, 3, \cdots, N_t; N_t = N_c + N_a) \tag{15}$$

The symbol q denotes the penalty parameter and the value of $q = 3$ will be used as in Kim and Kim (2014) and Kang et al. (2016): It is convenient to define the following symbols:

$$\boldsymbol{\xi} = \{\xi_1, \xi_2, \cdots, \xi_{N_t}\}^T, \mathbf{k} = \{k_1, k_2, \cdots, k_{N_t}\}^T \tag{16}$$

It is shown in Kim and Kim (2014) that the correct DOF (degree-of-freedom) of a mechanism can be ensured if the mean energy transmittance efficiency function ($\overline{\eta}$) is maximized or 1-$\overline{\eta}$ is minimized. On the other hand, the desired path which is given without prescribed timing can be traced by checking the differences between the Fourier descriptors describing the desired path and those describing the generated path. So, we set up the following optimization problem for mechanism synthesis:

$$\begin{aligned} \underset{\xi\in\mathbf{R}^{N_t}}{\text{Minimize}} \quad & 1-\overline{\eta} \\ \text{subject to} \quad & C_0\left(\left|a_{0,gen}-a_{0,des}\right|-\varepsilon\right)\le 0 \\ & C_n\left(\left|a_{n,gen}-a_{n,des}\right|-\varepsilon\right)\le 0 \ (n=1,2,\cdots,p) \\ & S_n\left(\left|b_{n,gen}-b_{n,des}\right|-\varepsilon\right)\le 0 \ (n=1,2,\cdots,p) \\ & (\varepsilon : \text{small value of tolerance}) \end{aligned} \tag{17}$$

where

$$\overline{\eta}=\frac{1}{T}\sum_{t^*=1}^{T}\eta_{t^*} \quad (0\le\eta\le 1) \tag{18}$$

The energy transmittance efficiency function at each time step t^* (η_{t^*}) is defined as the ratio of the output work at the end-effector to the input work done by the input link:

$$\eta_{t^*}=\frac{W_{\text{out},t^*}}{W_{inp,t^*}}\left(t^*=1,2,\cdots,T\right) \tag{19}$$

By the principle of energy conservation, the input work $W_{t^*}^{inp}$ must be equal to the sum of the output work $W_{t^*}^{\text{out}}$ by the external force and the stored energy U_{t^*} in the system:

$$W_{inp,t^*}=W_{\text{out},t^*}+U_{t^*}\left(t^*=1,2,\cdots,T\right) \tag{20}$$

Therefore, (19) can be rewritten as

$$\eta_{t^*}=\frac{W_{\text{out},t^*}}{W_{inp,t^*}}=\frac{W_{\text{out},t^*}}{W_{inp,t^*}+U_{t^*}}\left(t^*=1,2,\cdots,T\right) \tag{21}$$

The output work W_{out,t^*} can be defined as

$$W_{\text{out},t^*}=\sum_{t=1}^{t^*}\mathbf{F}_{ext,t}\cdot\left(\mathbf{r}_{Q,t-1}-\mathbf{r}_{Q,t}\right) \tag{22}$$

where $\mathbf{F}_{\text{ext},t}$ in (22) denotes the external force applied to the end-effector (Kim and Kim (2014) and Kang et al. (2016)). It is defined as

$$\mathbf{F}_{ext,t}=F_0\frac{\mathbf{r}_{Q,t-1}-\mathbf{r}_{Q,t}}{\left\|\mathbf{r}_{Q,t-1}-\mathbf{r}_{Q,t}\right\|} \tag{23}$$

With the definition (23), the external force is always applied against the motion of the end-effector. If $\mathbf{F}_{\text{ext},t}(F_0\neq 0)$ in (23) is introduced, output work and the energy transmittance efficiency function can be calculated. Then by minimizing $(1-\overline{\eta})$, the synthesized mechanism can have the correct degree of freedom as shown in Kim and Kim (2014).

The constraint equations in (17) involve the Fourier coefficients (a_0, a_n, b_n). The quantities with "gen" and "des" are related to the generated path of the end-effector of a mechanism in its current configuration and the desired path, respectively. The symbol ε is a user-defined tolerance while C_0, C_n and S_n are scaling factors introduced to facilitate convergence. Because the orders of magnitude of the objective function and the constraint equations (without the scaling factors) can be quite different, proper scaling of the constraint equations would help stable convergence. By noting that the objective function always varies between 0 and 1, the constraint equations are so scaled as to have the same order of magnitude as the objective function. Specifically, the following scaling is used for all case studies considered:

$$\begin{aligned} & C_0=C_n=S_n \\ & =\left(\max\left[\ \left|a_{0,gen}-a_{0,des}\right|,\left|a_{n,gen}-a_{n,des}\right|,\left|b_{n,gen}-b_{n,des}\right|\ \right]_{\text{at the 0th iteration}}\right)^{-1} \end{aligned} \tag{24}$$

4.2 Sensitivity analysis

To obtain the sensitivity of the objective function and the constraint equations in (17) with respect to the design variable $\boldsymbol{\xi}=\left\{\xi_1,\xi_2,\cdots,\xi_{N_t}\right\}^T$, we first calculate:

$$\begin{aligned} \frac{d\eta_{t^*}}{d\xi_i} &= \frac{d\mathbf{k}}{d\xi_i}\frac{d\eta_{t^*}}{d\mathbf{k}} \\ &= \frac{d\mathbf{k}}{d\xi_i}\left(\frac{\frac{dW_{\text{out},t^*}}{d\mathbf{k}}\left(W_{\text{out},t^*}+U_{t^*}\right)-W_{\text{out},t^*}\left(\frac{dW_{\text{out},t^*}}{d\mathbf{k}}+\frac{dU_{t^*}}{d\mathbf{k}}\right)}{\left(W_{\text{out},t^*}+U_{t^*}\right)^2}\right) \\ &= \frac{d\mathbf{k}}{d\xi_i}\left(\frac{\left(\frac{\partial W_{\text{out},t^*}}{\partial\mathbf{k}}+\frac{\partial W_{\text{out},t^*}}{\partial\mathbf{v}_{t^*}}\frac{\partial\mathbf{v}_{t^*}}{\partial\mathbf{k}}\right)}{\left(W_{\text{out},t^*}+U_{t^*}\right)}-\frac{W_{\text{out},t^*}\left(\frac{dW_{\text{out},t^*}}{d\mathbf{k}}+\left(\frac{\partial U_{t^*}}{\partial\mathbf{k}}+\frac{\partial U_{t^*}}{\partial\mathbf{v}_{t^*}}\frac{\partial\mathbf{v}_{t^*}}{\partial\mathbf{k}}\right)\right)}{\left(W_{\text{out},t^*}+U_{t^*}\right)^2}\right) \end{aligned} \tag{25}$$

with

$$\frac{d\mathbf{k}}{d\xi} = \mathrm{diag}\left(3k_{\max}(\xi_1)^2, 3k_{\max}(\xi_2)^2, \ldots, 3k_{\max}(\xi_{N_t})^2\right),$$
$$\frac{\partial \mathbf{v}_{t^*}}{\partial \mathbf{k}} = -\left\{\frac{\partial}{\partial \mathbf{v}_{t^*}}\left(\frac{\partial U_{t^*}}{\partial \mathbf{v}_{t^*}}\right)\right\}^{-1}\left\{\frac{\partial}{\partial \mathbf{k}}\left(\frac{\partial U_{t^*}}{\partial \mathbf{v}_{t^*}}\right)\right\}$$

The partial derivative $\partial U_{t^*}/\partial \mathbf{k}$ of the internal strain energy of the spring coefficients can be obtained easily from (4). Note that the partial derivative $\partial W_{\mathrm{out},t^*}/\partial \mathbf{k}$ of the work performed by the external force of the spring coefficients is zero.

The sensitivity of the constraint equations in (17) can be expressed as

$$\begin{aligned}
\frac{d\left(C_0\left(\left|a_{0,gen}-a_{0,des}\right|-\varepsilon\right)\right)}{d\xi} &= \frac{C_0\left(a_{0,gen}-a_{0,des}\right)}{\left|a_{0,gen}-a_{0,des}\right|}\frac{da_{0,gen}}{d\xi},\\
\frac{d\left(C_n\left(\left|a_{n,gen}-a_{n,des}\right|-\varepsilon\right)\right)}{d\xi} &= \frac{C_n\left(a_{n,gen}-a_{n,des}\right)}{\left|a_{n,gen}-a_{n,des}\right|}\frac{da_{n,gen}}{d\xi},\\
\frac{d\left(S_n\left(\left|b_{n,gen}-b_{n,des}\right|-\varepsilon\right)\right)}{d\xi} &= \frac{S_n\left(b_{n,gen}-b_{n,des}\right)}{\left|b_{n,gen}-b_{n,des}\right|}\frac{db_{n,gen}}{d\xi},
\end{aligned} \tag{26}$$

and the derivatives of the Fourier coefficients can be expressed as

$$\begin{aligned}
\frac{da_{0,gen}}{d\xi} &= \frac{d\mathbf{k}}{d\xi}\frac{da_{0,gen}}{d\mathbf{k}} = \frac{d\mathbf{k}}{d\xi}\left(\frac{\partial a_{0,gen}}{\partial \mathbf{k}} + \frac{\partial a_{0,gen}}{\partial \mathbf{v}_{t^*}}\frac{\partial \mathbf{v}_{t^*}}{\partial \mathbf{k}}\right),\\
\frac{da_{n,gen}}{d\xi} &= \frac{d\mathbf{k}}{d\xi}\frac{da_{n,gen}}{d\mathbf{k}} = \frac{d\mathbf{k}}{d\xi}\left(\frac{\partial a_{n,gen}}{\partial \mathbf{k}} + \frac{\partial a_{n,gen}}{\partial \mathbf{v}_{t^*}}\frac{\partial \mathbf{v}_{t^*}}{\partial \mathbf{k}}\right),\\
\frac{db_{n,gen}}{d\xi} &= \frac{d\mathbf{k}}{d\xi}\frac{db_{n,gen}}{d\mathbf{k}} = \frac{d\mathbf{k}}{d\xi}\left(\frac{\partial b_{n,gen}}{\partial \mathbf{k}} + \frac{\partial b_{n,gen}}{\partial \mathbf{v}_{t^*}}\frac{\partial \mathbf{v}_{t^*}}{\partial \mathbf{k}}\right)
\end{aligned} \tag{27}$$

The Fourier descriptors of the generated path, $a_{0,gen}$, $a_{n,gen}$ and $b_{n,gen}$, are the functions of the coordinates of the block center to which the end-effector is attached ($\mathbf{r}_{Q,t^*}$). So, the derivatives of the Fourier descriptors by the spring stiffness coefficients ($\partial a_{0,gen}/\partial \mathbf{k}$, $\partial a_{n,gen}/\partial \mathbf{k}$ and $\partial b_{n,gen}/\partial \mathbf{k}$) become zero. Also, by the same reason, $\left(\partial a_{0,gen}/\partial \mathbf{v}_{t^*}, \partial a_{n,gen}/\partial \mathbf{v}_{t^*}\right.$ and $\left.\partial b_{n,gen}/\partial \mathbf{v}_{t^*}\right)$ can be obtained by using $\left(\partial a_{0,gen}/\partial \mathbf{r}_{Q,t^*}, \partial a_{n,gen}/\partial \mathbf{r}_{Q,t^*}\right.$ and $\left.\partial b_{n,gen}/\partial \mathbf{r}_{Q,t^*}\right)$ because the others are all zero.

The explicit expressions for $\partial a_{0,gen}/\partial \mathbf{r}_{Q,t^*}$, $\partial a_{n,gen}/\partial \mathbf{r}_{Q,t^*}$ and $\partial b_{n,gen}/\partial \mathbf{r}_{Q,t^*}$ can be obtained by the chain rule, and the results are given below:

$$\begin{aligned}
\frac{\partial a_{0,gen}}{\partial \mathbf{r}_{Q,t^*}} &= \left[\frac{\partial a_{0,gen}}{\partial x_{Q,t^*}}, \frac{\partial a_{0,gen}}{\partial y_{Q,t^*}}\right]^T,\\
\frac{\partial a_{n,gen}}{\partial \mathbf{r}_{Q,t^*}} &= \left[\frac{\partial a_{n,gen}}{\partial x_{Q,t^*}}, \frac{\partial a_{n,gen}}{\partial y_{Q,t^*}}\right]^T, \frac{\partial b_{n,gen}}{\partial \mathbf{r}_{Q,t^*}} = \left[\frac{\partial b_{n,gen}}{\partial x_{Q,t^*}}, \frac{\partial b_{n,gen}}{\partial y_{Q,t^*}}\right]^T
\end{aligned} \tag{28}$$

$$\begin{aligned}
\frac{\partial a_{0,gen}}{\partial x_{Q,t^*}} &= \sum_{t=1}^{T}\left\{\frac{\partial f\left(\tilde{s}_t\right)}{\partial x_{Q,t^*}}\Delta\tilde{s}_t + f\left(\tilde{s}_t\right)\frac{\partial \Delta\tilde{s}_t}{\partial x_{Q,t}}\right\}, \frac{\partial a_{0,gen}}{\partial y_{Q,t^*}} = \sum_{t=1}^{T}\left\{\frac{\partial f\left(\tilde{s}_t\right)}{\partial y_{Q,t^*}}\Delta\tilde{s}_t + f\left(\tilde{s}_t\right)\frac{\partial \Delta\tilde{s}_t}{\partial y_{Q,t^*}}\right\}\\
\frac{\partial a_{n,gen}}{\partial x_{Q,t^*}} &= 2\sum_{t=1}^{T}\left\{\begin{array}{c}\frac{\partial f\left(\tilde{s}_t\right)}{\partial x_{Q,t^*}}\cos\left(2n\pi\tilde{s}_t\right)\Delta\tilde{s}_t - f\left(\tilde{s}_t\right)\sin\left(2n\pi\tilde{s}_t\right)\left(2n\pi\frac{\partial \tilde{s}_t}{\partial x_{Q,t^*}}\right)\Delta\tilde{s}_t\\ +f\left(\tilde{s}_t\right)\cos\left(2n\pi\tilde{s}_t\right)\frac{\partial \Delta\tilde{s}_t}{\partial x_{Q,t^*}}\end{array}\right\}\\
\frac{\partial a_{n,gen}}{\partial y_{Q,t^*}} &= 2\sum_{t=1}^{T}\left\{\begin{array}{c}\frac{\partial f\left(\tilde{s}_t\right)}{\partial y_{Q,t^*}}\cos\left(2n\pi\tilde{s}_t\right)\Delta\tilde{s}_t - f\left(\tilde{s}_t\right)\sin\left(2n\pi\tilde{s}_t\right)\left(2n\pi\frac{\partial \tilde{s}_t}{\partial y_{Q,t^*}}\right)\Delta\tilde{s}_t\\ +f\left(\tilde{s}_t\right)\cos\left(2n\pi\tilde{s}_t\right)\frac{\partial \Delta\tilde{s}_t}{\partial y_{Q,t^*}}\end{array}\right\}\\
\frac{\partial b_{n,gen}}{\partial x_{Q,t^*}} &= 2\sum_{t=1}^{T}\left\{\begin{array}{c}\frac{\partial f\left(\tilde{s}_t\right)}{\partial x_{Q,t^*}}\sin\left(2n\pi\tilde{s}_t\right)\Delta\tilde{s}_t + f\left(\tilde{s}_t\right)\cos\left(2n\pi\tilde{s}_t\right)\left(2n\pi\frac{\partial \tilde{s}_t}{\partial x_{Q,t^*}}\right)\Delta\tilde{s}_t\\ +f\left(\tilde{s}_t\right)\sin\left(2n\pi\tilde{s}_t\right)\frac{\partial \Delta\tilde{s}_t}{\partial x_{Q,t^*}}\end{array}\right\}\\
\frac{\partial b_{n,gen}}{\partial y_{Q,t^*}} &= 2\sum_{t=1}^{T}\left\{\begin{array}{c}\frac{\partial f\left(\tilde{s}_t\right)}{\partial y_{Q,t^*}}\sin\left(2n\pi\tilde{s}_t\right)\Delta\tilde{s}_t + f\left(\tilde{s}_t\right)\cos\left(2n\pi\tilde{s}_t\right)\left(2n\pi\frac{\partial \tilde{s}_t}{\partial y_{Q,t^*}}\right)\Delta\tilde{s}_t\\ +f\left(\tilde{s}_t\right)\sin\left(2n\pi\tilde{s}_t\right)\frac{\partial \Delta\tilde{s}_t}{\partial y_{Q,t^*}}\end{array}\right\}
\end{aligned} \tag{29}$$

$$\frac{\partial f\left(\tilde{s}_t\right)}{\partial x_{Q,t^*}}=\begin{cases}\dfrac{\left(x_{Q,t}-x_c\right)-\left(x_{Q,t}-x_c\right)\dfrac{\partial x_c}{\partial x_{Q,t^*}}-\left(y_{Q,t}-y_c\right)\dfrac{\partial y_c}{\partial x_{Q,t^*}}}{\sqrt{\left(x_{Q,t}-x_c\right)^2+\left(y_{Q,t}-y_c\right)^2}} & \left(t=t^*\right)\\ -\dfrac{\left(x_{Q,t}-x_c\right)\dfrac{\partial x_c}{\partial x_{Q,t^*}}+\left(y_{Q,t}-y_c\right)\dfrac{\partial y_c}{\partial x_{Q,t^*}}}{\sqrt{\left(x_{Q,t}-x_c\right)^2+\left(y_{Q,t}-y_c\right)^2}} & \left(t\neq t^*\right)\end{cases}$$

$$\frac{\partial f\left(\tilde{s}_t\right)}{\partial y_{Q,t^*}}=\begin{cases}\dfrac{\left(y_{Q,t}-y_c\right)-\left(x_{Q,t}-x_c\right)\dfrac{\partial x_c}{\partial y_{Q,t^*}}-\left(y_{Q,t}-y_c\right)\dfrac{\partial y_c}{\partial y_{Q,t^*}}}{\sqrt{\left(x_{Q,t}-x_c\right)^2+\left(y_{Q,t}-y_c\right)^2}} & \left(t=t^*\right)\\ -\dfrac{\left(x_{Q,t}-x_c\right)\dfrac{\partial x_c}{\partial y_{Q,t^*}}+\left(y_{Q,t}-y_c\right)\dfrac{\partial y_c}{\partial y_{Q,t^*}}}{\sqrt{\left(x_{Q,t}-x_c\right)^2+\left(y_{Q,t}-y_c\right)^2}} & \left(t\neq t^*\right)\end{cases} \tag{30}$$

$$\begin{aligned}&\frac{\partial x_c}{\partial x_{Q,t^*}}=\frac{1}{2}\left(\Delta\tilde{s}_{t^*}+\Delta\tilde{s}_{t^*+1}\right)+\sum_{t=1}^{T}\frac{x_{Q,t+1}+x_{Q,t}}{2}\frac{\partial\Delta\tilde{s}_t}{\partial x_{Q,t^*}},\ \frac{\partial x_c}{\partial y_{Q,t^*}}=\sum_{t=1}^{T}\frac{x_{Q,t+1}+x_{Q,t}}{2}\frac{\partial\Delta\tilde{s}_t}{\partial y_{Q,t^*}},\\ &\frac{\partial y_c}{\partial x_{Q,t^*}}=\sum_{t=1}^{T}\frac{y_{Q,t+1}+y_{Q,t}}{2}\frac{\partial\Delta\tilde{s}_t}{\partial x_{Q,t^*}},\ \frac{\partial y_c}{\partial y_{Q,t^*}}=\frac{1}{2}\left(\Delta\tilde{s}_{t^*}+\Delta\tilde{s}_{t^*+1}\right)+\sum_{t=1}^{T}\frac{y_{Q,t+1}+y_{Q,t}}{2}\frac{\partial\Delta\tilde{s}_t}{\partial y_{Q,t^*}}\end{aligned} \tag{31}$$

$$\frac{\partial\Delta\tilde{s}_t}{\partial x_{Q,t^*}}=\frac{\partial\Delta s_t}{\partial x_{Q,t^*}}\frac{1}{L}-\frac{\Delta s_t}{L^2}\frac{\partial L}{\partial x_{Q,t^*}},\quad \frac{\partial\Delta\tilde{s}_t}{\partial y_{Q,t^*}}=\frac{\partial\Delta s_t}{\partial y_{Q,t^*}}\frac{1}{L}-\frac{\Delta s_t}{L^2}\frac{\partial L}{\partial y_{Q,t^*}} \tag{32}$$

with

$$\frac{\partial s_t}{\partial x_{Q,t^*}}=\sum_{j=1}^{t}\frac{\partial\Delta s_t}{\partial x_{Q,t^*}},\quad \frac{\partial s_t}{\partial y_{Q,t^*}}=\sum_{j=1}^{t}\frac{\partial\Delta s_t}{\partial y_{Q,t^*}}$$

$$\frac{\partial\Delta s_t}{\partial x_{Q,t^*}}=\begin{cases}\dfrac{-\left(x_{Q,t^*+1}-x_{Q,t^*}\right)}{\sqrt{\left(x_{Q,t^*+1}-x_{Q,t^*}\right)^2+\left(y_{Q,t^*+1}-y_{Q,t^*}\right)^2}} & \left(t=t^*\right)\\ \dfrac{\left(x_{Q,t^*}-x_{Q,t^*-1}\right)}{\sqrt{\left(x_{Q,t^*}-x_{Q,t^*-1}\right)^2+\left(y_{Q,t^*}-y_{Q,t^*-1}\right)^2}} & \left(t=t^*-1\right)\\ 0 & \left(t\neq t^*-1,t\neq t^*\right)\end{cases}$$

$$\frac{\partial\Delta s_t}{\partial y_{Q,t^*}}=\begin{cases}\dfrac{-\left(y_{Q,t^*+1}-y_{Q,t^*}\right)}{\sqrt{\left(x_{Q,t^*+1}-x_{Q,t^*}\right)^2+\left(y_{Q,t^*+1}-y_{Q,t^*}\right)^2}} & \left(t=t^*\right)\\ \dfrac{\left(y_{Q,t^*}-y_{Q,t^*-1}\right)}{\sqrt{\left(x_{Q,t^*}-x_{Q,t^*-1}\right)^2+\left(y_{Q,t^*}-y_{Q,t^*-1}\right)^2}} & \left(t=t^*-1\right)\\ 0 & \left(t\neq t^*-1,t\neq t^*\right)\end{cases} \tag{33}$$

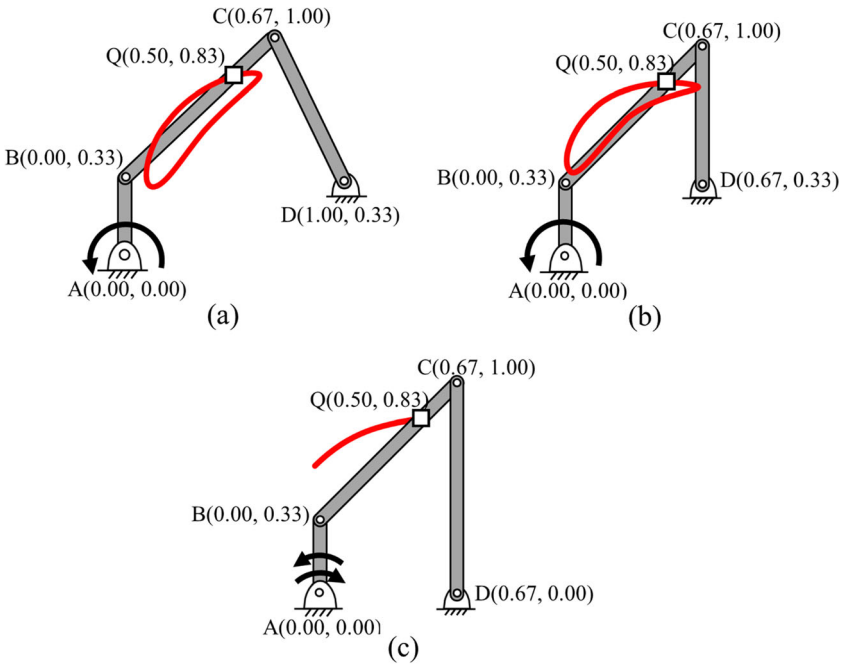

Fig. 6 The target paths (red solid lines passing through Q) generated by reference mechanisms. The curves passing through open squares that represent the end-effectors are the target paths. Input links are those connecting points A and B. The shapes of (a) a banana (Case Study 1), (b) a banana with a cusp (Case Study 2), and (c) an elliptical arc (Case Study 3) are considered

$$\frac{\partial L}{\partial x_{Q,t^*}} = \frac{-\left(x_{Q,t^*+1} - \partial_x Q, t^*\right)}{\sqrt{\left(x_{Q,t^*+1} - x_{Q,t^*}\right)^2 + \left(y_{Q,t^*+1} - y_{Q,t^*}\right)^2}} + \frac{\left(x_{Q,t^*} - x_{Q,t^*-1}\right)}{\sqrt{\left(x_{Q,t^*} - x_{Q,t^*-1}\right)^2 + \left(y_{Q,t^*} - y_{Q,t^*-1}\right)^2}}$$
$$\frac{\partial L}{\partial y_{Q,t^*}} = \frac{-\left(y_{Q,t^*+1} - y_{Q,t^*}\right)}{\sqrt{\left(x_{Q,t^*+1} - x_{Q,t^*}\right)^2 + \left(y_{Q,t^*+1} - y_{Q,t^*}\right)^2}} + \frac{\left(y_{Q,t^*} - y_{Q,t^*-1}\right)}{\sqrt{\left(x_{Q,t^*} - x_{Q,t^*-1}\right)^2 + \left(y_{Q,t^*} - y_{Q,t^*-1}\right)^2}} \tag{34}$$

5 Case studies

In this section, four different types of case studies will be considered to demonstrate the effectiveness of the proposed formulation given in Section 4. Here, we will consider the recovery of the reference mechanisms generating specific paths but the paths will be given without specific timing in our formulation.

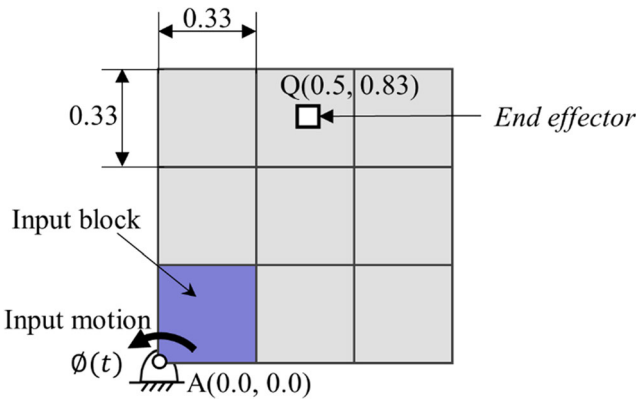

Fig. 7 The SBM (spring-connected rigid block model) used to discretize the design domain

Figure 6 shows three reference mechanisms and the target paths generated by them. The reason for choosing the paths as shown in Fig. 6 will be explained later when the specific problem is solved. To synthesize mechanisms to generate the paths shown in Fig. 6, the Fourier descriptors are used for path representation. The design domain is discretized into 3×3 rigid blocks. Its dimensions are shown in Fig. 7. For the used discretization, N_t=60 (N_t: the total number of the design variables), N_c=24, and N_a=36. Note that there is no spring element prescribed at Node A because Node A is used as a hinge point needed to drive the circular motion of the input link, Link AB.

As we solve the four synthesis problems, we will investigate various aspects, such as convergence, the effects of the number of Fourier harmonics, etc. To update the design variables ξ for the proposed topology optimization of mechanisms, the method of moving asymptotes (MMA) (Svanberg 1987), a gradient-based optimizer, is used.

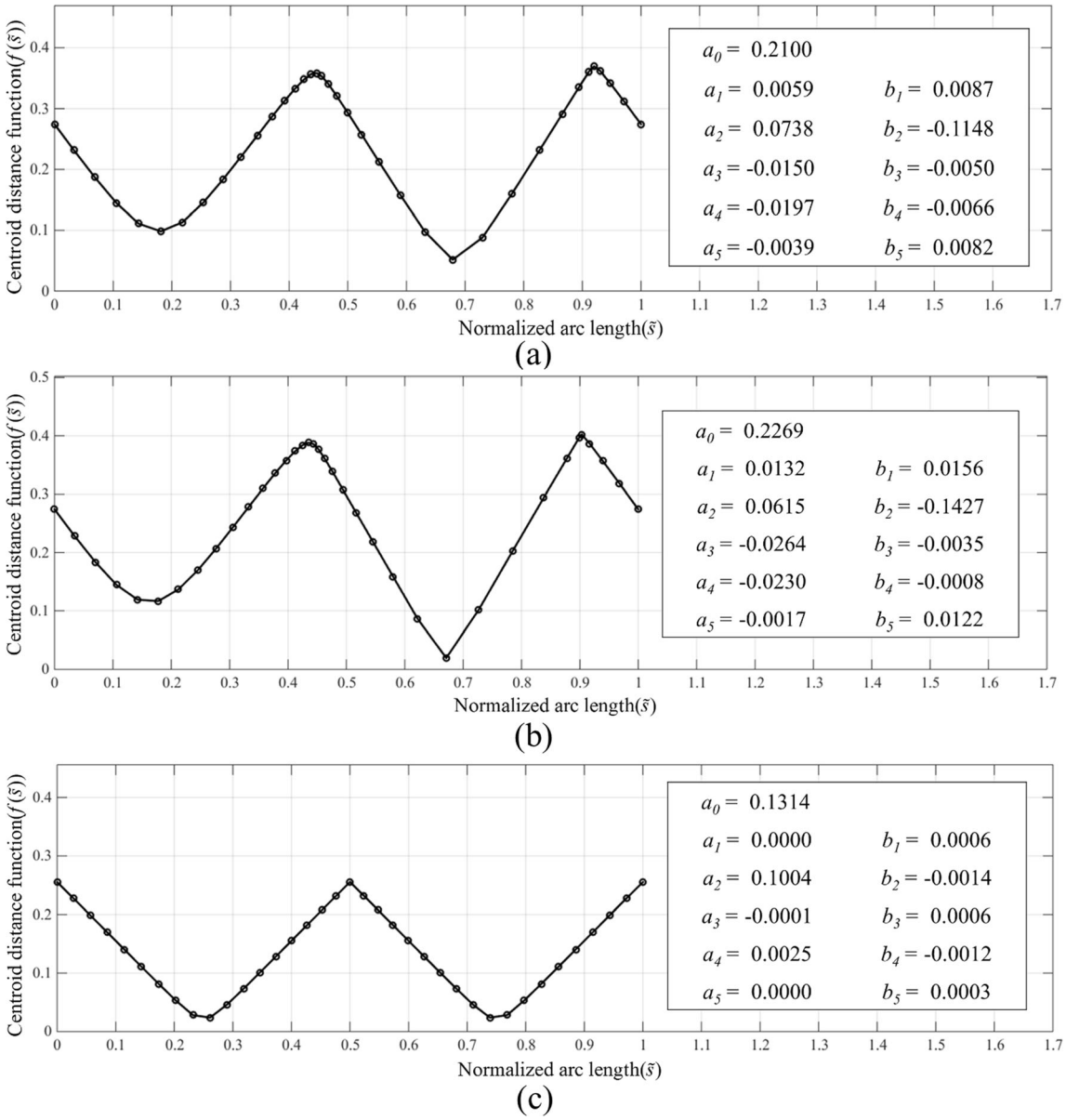

Fig. 8 (a,b,c) The centroid distance functions for the end-effector paths shown in Fig. 6(a,b,c), respectively

5.1 Case study 1 – path shape of a banana

This problem considers the synthesis of a mechanism to generate the banana shaped curve illustrated in Fig. 6(a). The input motion is described by the rotation angle of the input link *AB* in 36 steps so that the input link *AB* is rotated by 10° per each step. Thus, the angle of rotation of the input link can be expressed as

$$\phi_{des,t} = \phi_{gen,t} = \frac{\pi}{18} t (t = 1, 2, \cdots, 36)$$

To express the path of the end-effector shown in Fig. 6(a) as the centroid distance function $f(\tilde{s})$ $p = 5$ is used in its Fourier series expansion. The function $f(\tilde{s})$ is plotted in Fig. 8(a) with the Fourier series coefficients. The effects of the number of the Fourier descriptors will be discussed later in more details with another case study.

The intermediate and final mechanism layouts obtained by using the formulation, (17), are shown in Fig. 9(a). Figure 9(b) shows that the energy transmittance efficiency $\overline{\eta}$ reaches almost 1 (the maximum value to be attained) at the iteration number $n_{iter} = 40$, indicating that the correct DOF equal to 1 is acquired. Also, the all constraints stated in (17) remain to be satisfied after $n_{iter} = 40$. The values of the design variables at the convergence are plotted in Fig. 9(c). It shows that most of the spring stiffness values reaches their bound values. (Note that after intermediate values were post-processed to $k_{\max}$ or $k_{\min}$ for linkage identification, the values of the objective function and the constraint functions were little changed.) The springs for $33 \leq m \leq 36$ in Fig. 9(c) are the anchoring springs.

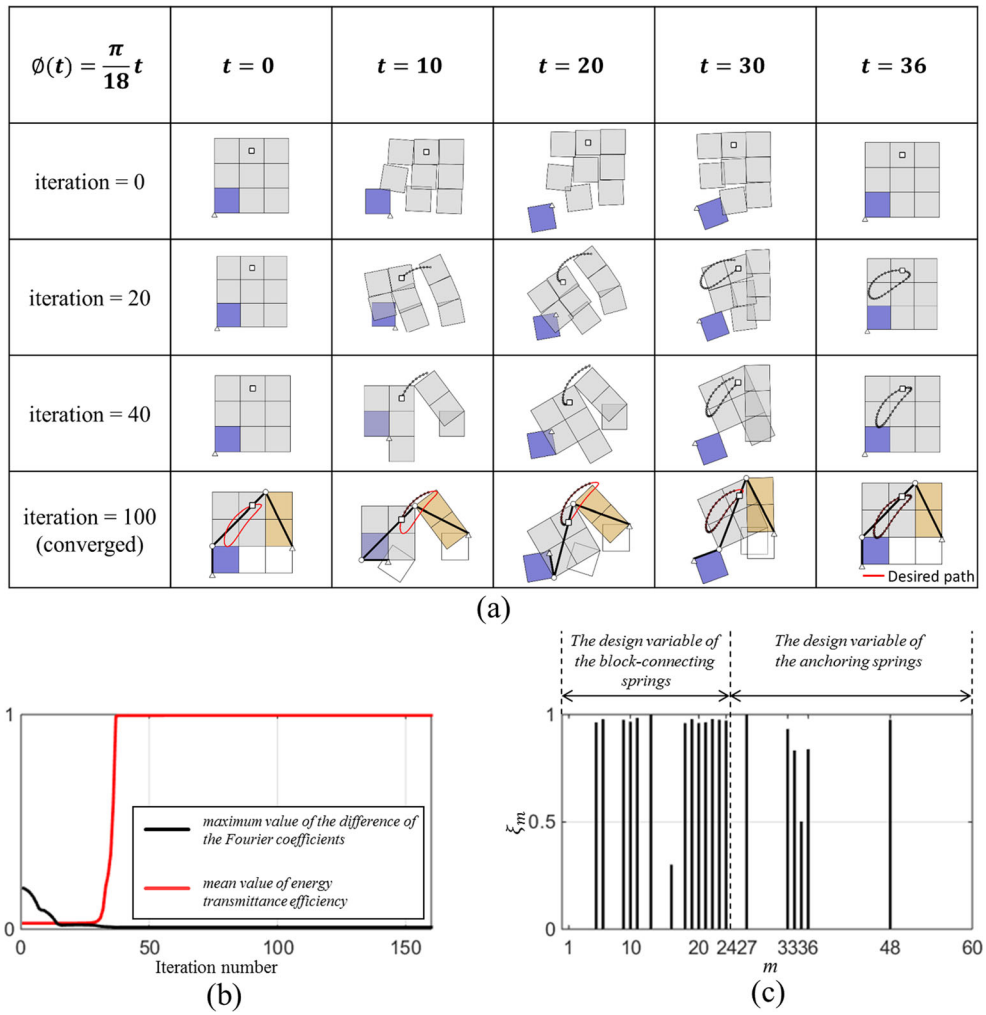

Fig. 9 The results obtained for the curve shape of a banana given in Fig. 6(a). (a) Intermediate and final layouts at different time steps, (b) the iteration history of the objective function and the constraint equations, and (c) the converged stiffness values of the zero-length springs. In (a), the solid lines (in black) that pass through the end-effector (marked with open squares) denote the actual paths of the mechanism being synthesized

In fact, they serve to anchor the right white block shown in Fig. 9(a) to the ground (after $n_{iter} = 100$) although not all of the stiffness values reached their maximum value. To identify the final optimized linkage configuration, one can simply check the spring stiffness values of the converged SBM as done in Nam et al. (2012), Kang et al. (2016) and Kim et al. (2007). More directly, one can identify the linkage configuration from the final SBM at an intermediate time step, say at $t = 10$ and it can be found that the resulting linkage mechanism is exactly the same as the reference linkage that generates the target path. This confirms that the proposed formulation successfully found the desired linkage mechanism.

5.2 Case study 2 – path shape of a banana with a cusp

The purpose of this example is to see if the proposed method can find a mechanism generating a path having an extreme shape feature, a cusp. Specifically, we consider a banana path shape with a cusp. The reference mechanism is shown in Fig. 6(b). All other conditions needed for the optimization are the same as those used for Case Study 1.

Figure 10(a) shows the intermediate and final linkage mechanism layouts. It shows that the desired mechanism that traces the target path is found by using the proposed optimization approach. The iteration history of the mean energy transmittance efficiency $\overline{\eta}$ is shown in Fig. 10(b). In fact, $\overline{\eta}$ reached almost 1 after $n_{iter} = 60$, indicating slower convergence than in Case Study 1. From Fig. 10(c), one can see that three design variables related to the anchoring springs have the maximum value although there are two ground positions. This means that two anchoring springs among the three springs make the same ground joint.

5.3 Case study 3 – Path shape of an elliptical arc

As Case Study 3, we consider the synthesis of a mechanism the end-effector of which traces an arc of an elliptical curve. Because the overall solution behavior for this problem is similar to that considered for Case Study 1, we aim to focus mainly on how much the convergence behavior is affected by the number of the Fourier harmonics employed for the representation of the target path. In this problem, the input

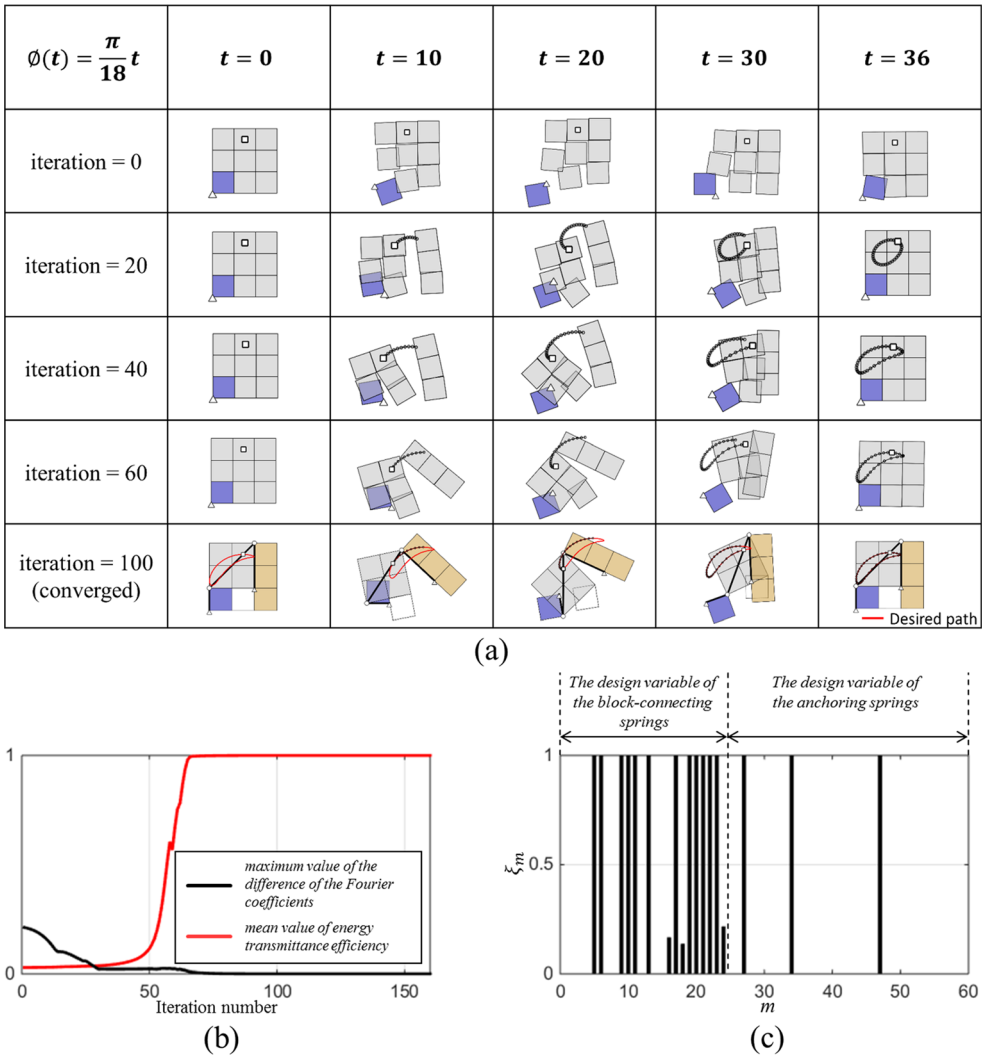

Fig. 10 The results obtained for the curve shape of a banana with a cusp given in Fig. 6(b). (a) Intermediate and final layouts at different time steps, (b) the iteration history of the objective function and the constraint equations, and (c) the converged stiffness values of the zero-length springs. In (a), the solid lines (in black) that pass through the end-effector (marked with open squares) denote the actual paths of the mechanism being synthesized

motion to the system is set as a reciprocating motion that makes the given open path as if it were a closed path (Buśkiewicz 2010). Therefore, the Fourier series representation useful for periodic functions can be directly applicable. In this representation, the starting and ending points of the path describing a reciprocal motion become the same.

For numerical calculations, the target path is obtained by rotating the input linkage counterclockwise by 5° per step and, after 18 steps, the input linkage is rotated clockwise by the same number of steps. Thus, the angle of the input link can be expressed as

$$\phi_{des,t} = \phi_{gen,t} = \left\{ \begin{array}{c} \frac{\pi}{36}t \quad (t = 1, 2, \cdots, 18) \\ \frac{\pi}{36}(36-t)(t = 19, 20, \cdots, 36) \end{array} \right\}$$

The optimized results with $p = 4$ and $p = 5$ (p: the highest harmonic number in (13)) are shown in Fig. 11(a) and (b), respectively. The results show that the two optimized layouts are identical. Although not shown here, it was not possible to synthesize the correct mechanism when $p = 3$, indicating that a centroid distance function should be sufficiently accurately represented in order to find meaningful results. The previous study which used the Fourier descriptors and the centroid distance function for the shape optimization of linkage mechanisms also reported similar findings that the use of $p = 4$ to $p = 6$ is appropriate when the number of points to describe a centroid distance function is around 20 to 40 (Buśkiewicz 2010). In this problem, we used 36 points to describe the function and our finding is consistent with the result in Buśkiewicz (2010).

5.4 Case study 4 – revisit case study 1

As the last example, we revisit Case Study 1. Compared with the problem defined in Case Study 1, there are two differences. Firstly, the desired path illustrated in Fig. 12(a) for Case Study 4 is translated and rotated with respect to the one given in Fig. 6(a) for Case Study 1. Secondly, 50 data points are randomly selected for Case Study 4 (see the selected points

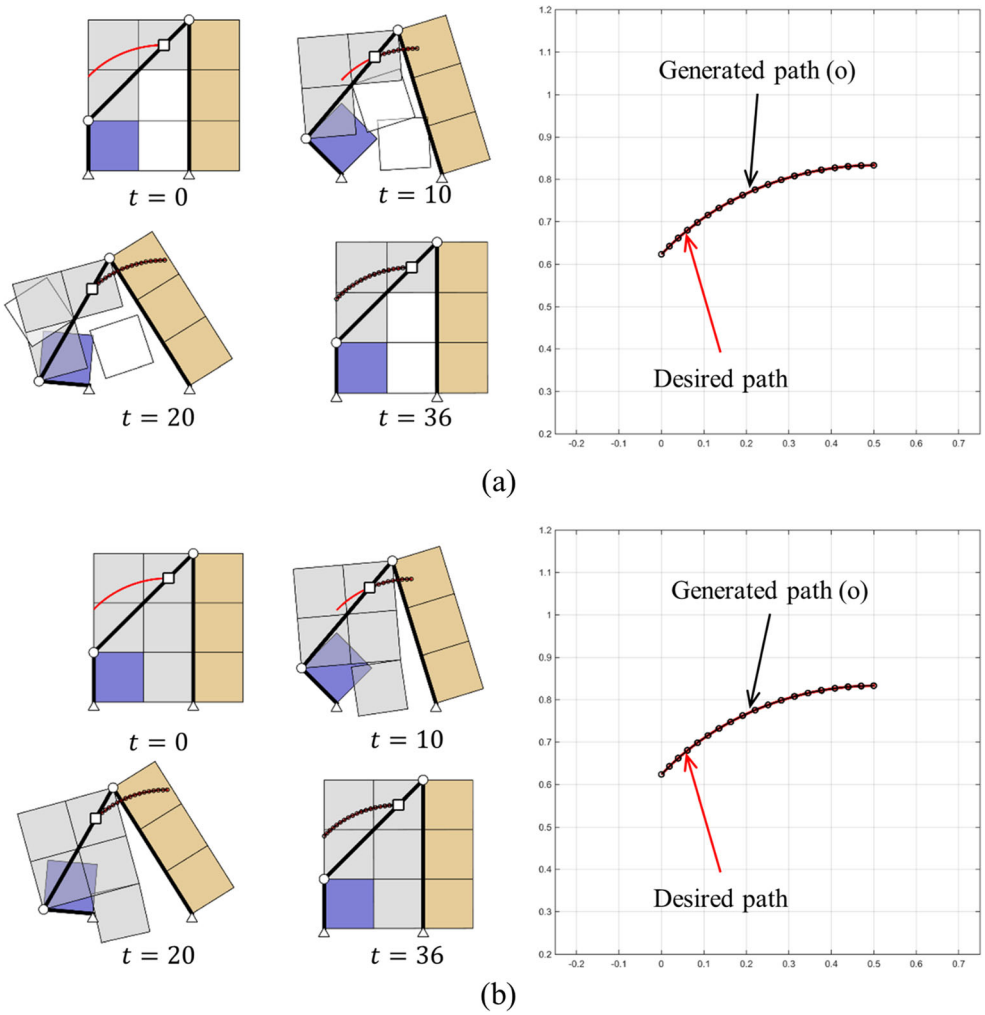

Fig. 11 The synthesized results for a mechanism generating the arc of an ellipse at its end-effector when the highest term in the Fourier series is equal to (a) $p = 4$ and (b) $p = 5$

marked on the desired path shown in Fig. 12(b)) out of 360 data points that are obtained by rotating the input link of the reference linkage in Fig. 6(a). This case study is considered to show that our formulation using the Fourier descriptors of the centroid distance functions works even if the path is described without specific timing. The number of data points as well as the timing of the desired path for Case Study 1 and Case Study 4 are different. If our formulation works, the same mechanism obtained for Case Study 1 should be obtained.

The synthesized result is shown in Fig. 12(a) and the iteration history is given in Fig. 12(c). As seen from Fig. 12(a), a mechanism is successfully synthesized even though the desired path has a different pose from that of the generated path. When the desired and generated paths are superposed after some translation and rotation, they virtually overlap. Also, the data points used to compute the Fourier coefficients for the generated path are different from those used to generate the desired path, as illustrated in Fig. 12(b). Nevertheless, the proposed method yielded the desired mechanism successfully. This problem cannot be solved if the structural error is directly minimized because the input timing for the mechanism during synthesis differs from the timing of the given data points and the poses of the desired and generated paths are different. Figure 12(d) compares the centroid distance functions of the desired path and the generated path approximated by the Fourier descriptors.

6 Conclusions

This study aimed to develop a topology optimization formulation for the automated synthesis of planar linkage mechanisms that generate desired path shapes without prescribed timing. While earlier topology optimization of linkage mechanisms were only concerned with prescribed timing problems, this study solved unprescribed timing problems for the first time.

When a desired path of the end-effector of a mechanism is given without specific timing, the path should be described by its shape, not by its locations at specific times. In this study, the shape was described by the centroid distance function. We employed this function for path description because paths can

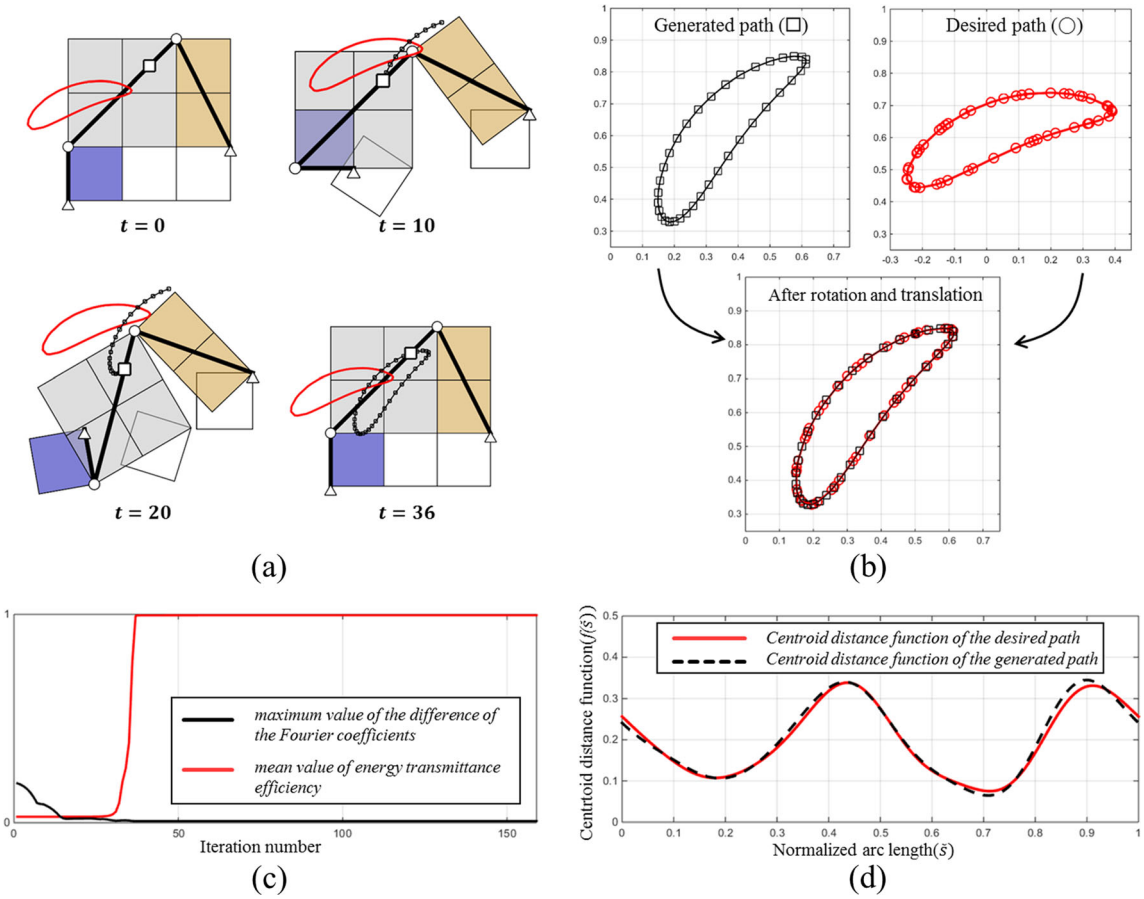

Fig. 12 Mechanism synthesis for a target banana-shaped path with different pose and sampling data points compared with the path given in Case Study 1. (a) The synthesized results, (b) the comparison of the desired and generated paths, (c) the iteration history, and (d) the comparison of the centroid distance functions of the desired and generated paths after convergence

be regarded to have the same shape curve regardless of their orientations and absolute locations as long as their centroid distance functions are the same. The centroid distance function was then expressed in Fourier series to avoid the dependence of the data point sampling for the representation of the centroid distance function, i.e., prescribed timing dependence. Its Fourier series coefficients are used as the shape descriptors of the path. To make the end-effector of the synthesized mechanism trace the target path, the constraint equations using the Fourier descriptors were specified. To utilize a gradient-based optimizer for the proposed topology optimization, the sensitivity analysis of the constraint equations involving the Fourier descriptors was analytically performed. The correct DOF was acquired by maximizing the energy transmittance efficiency function.

Several numerical case studies supported the effectiveness of the proposed method. In particular, the proposed formulation successfully synthesized a mechanism generating the desired path even if the generated path traces a path that was translated and rotated from the given path. The numerical examples considered in this study showed the advantage of using the Fourier descriptors of the centroid distance function because the synthesized results are not much affected by the selected data points used to describe the centroid distance function of the desired path. In order to synthesize more advanced, realistic mechanisms that can generate more complicated curves, the use of more blocks (finer mesh) with a more efficient and stable numerical solver may be needed. Also, one may need to consider simultaneous shape and topology optimization towards this direction. In either extension, the formulation developed here is expected to be employed. Also, the present formulation could be used for the synthesis of multi-DOF mechanisms yielding the desired workspace, which can be an interesting future research topic.

Acknowledgments This work was supported by the National Research Foundation of Korea (NRF) funded by the Ministry of Science, ICT & Future Planning, Korea (Numbers: 2016R1A2B3010231) contracted through IAMD (Institute of Advanced Machines and Design) at Seoul National University.

References

Bazan C, Barba DT, Blomgren P, Paolini P (2009) Image processing techniques for assessing contractility in isolated adult cardiac myocytes. J Biomed Imaging 2009(32):1–11

Buśkiewicz J (2010) Use of shape invariants in optimal synthesis of geared five-bar linkage. Mech Mach Theory 45(2):273–290

Buśkiewicz J, Starosta R, Walczak T (2009) On the application of the curve curvature in path synthesis. Mech Mach Theory 44(6):1223–1239

Granlund GH (1972) Fourier preprocessing for hand print character recognition. IEEE Trans Comput 21(2):195–201

Huang C-L, Huang D-H (1998) A content-based image retrieval system. Image Vis Comput 16(3):149–163

Kang SW, Kim SI, Kim YY (2016) Topology optimization of planar linkage systems involving general joint types. Mech Mach Theory 104:130–160

Kauppinen H, Seppanen T, Pietikainen M (1995) An experimental comparison of autoregressive and Fourier-based descriptors in 2D shape classification. IEEE Trans Pattern Anal Mach Intell 17(2):201–207

Kawamoto A (2005) Path-generation of articulated mechanisms by shape and topology variations in non-linear truss representation. Int J Numer Methods Eng 64(12):1557–1574

Kawamoto A, Bendsøe MP, Sigmund O (2004a) Articulated mechanism design with a degree of freedom constraint. Int J Numer Methods Eng 61(9):1520–1545

Kawamoto A, Bendsøe MP, Sigmund O (2004b) Planar articulated mechanism design by graph theoretical enumeration. Struct Multidiscip Optim 27(4):295–299

Kim BS, Yoo HH (2014) Unified mechanism synthesis method of a planar four-bar linkage for path generation employing a spring-connected arbitrarily sized rectangular block model. Multibody Syst Dyn 31(3):241–256

Kim SI, Kim YY (2014) Topology optimization of planar linkage mechanisms. Int J Numer Methods Eng 98(4):265–286

Kim YY, Jang G-W, Park JH, Hyun JS, Nam SJ (2007) Automatic synthesis of a planar linkage mechanism with revolute joints by using spring-connected rigid block models. J Mech Des 129(9):930–940

Lu G, Sajjanhar A (1999) Region-based shape representation and similarity measure suitable for content-based image retrieval. Multimedia Systems 7(2):165–174

Mehtre BM, Kankanhalli MS, Lee WF (1997) Shape measures for content based image retrieval: a comparison. Inf Process Manag 33(3):319–337

Nam SJ, Jang G-W, Kim YY (2012) The spring-connected rigid block model based automatic synthesis of planar linkage mechanisms: numerical issues and remedies. J Mech Des 134(5):051002

Ohsaki M, Nishiwaki S (2009) Generation of link mechanism by shape-topology optimization of trusses considering geometrical nonlinearity. J Comput Sci Technol 3(1):46–53

Persoon E, Fu K-S (1977) Shape discrimination using Fourier descriptors. IEEE Trans Syst Man Cybern 7(3):170–179

Rai AK, Saxena A, Mankame ND (2010) Unified synthesis of compact planar path-generating linkages with rigid and deformable members. Struct Multidiscip Optim 41(6):863–879

Rattan SS (2009) Theory of machines, 3rd edn. McGraw-Hill Higher Education, New Delhi

Sedlaczek K, Eberhard P (2009) Topology optimization of large motion rigid body mechanisms with nonlinear kinematics. J Comput Nonlinear Dyn 4(2):021011

Svanberg K (1987) The method of moving asymptotes—a new method for structural optimization. Int J Numer Methods Eng 24(2):359–373

Ullah I, Kota S (1997) Optimal synthesis of mechanisms for path generation using Fourier descriptors and global search methods. J Mech Des 119(4):504–510

Wu J, Ge QJ, Gao F (2009) An efficient method for synthesizing crank-rocker mechanisms for generating low harmonic curves. In: ASME Proceedings - 33rd Mechanisms and Robotics Conference, San Diego, California, USA, 2009. pp. DETC 2009–87140.

Wu J, Ge QJ, Gao F, Guo WZ (2011) On the extension of a Fourier descriptor based method for planar four-bar linkage synthesis for generation of open and closed paths. J Mech Robot 3(3):031002

Yang M, Kpalma K, Ronsin J (2008) A survey of shape feature extraction techniques. Peng-Yeng Yin Pattern Recognition, IN-TECH:43–90

Zahn CT, Roskies RZ (1972) Fourier descriptors for plane closed curves. IEEE Trans Comput 21(3):269–281

Zhang D, Lu G (2001) Content-based shape retrieval using different shape descriptors: a comparative study. In: IEEE International Conference on Multimedia and Expo, Japan, 2001. pp. 1139–1142